Published in final edited form as:
J Compos Mater. 2011 August ; 45(18): 1863–1872. doi:10.1177/0021998310388318.

Confined compression of dental composites for Class I restorations

Amol S. Patki, **Murat Vural**, and **Mike Gosz**
Department of Mechanical, Materials, and Aerospace Engineering, Illinois Institute of Technology, 10 West 32nd Street, Chicago, IL 60616, USA.

Abstract

This study focuses on the mechanical response of a particle-reinforced restorative dental composite (Renew™) under proportional transverse confinement to understand the effects of stress multiaxiality on its mechanical and failure behaviors. We describe the confining ring technique as an experimental tool to introduce multiaxial compressive stress states in dental composites that realistically mimic three-dimensional stress states commonly experienced by dental restorations in the oral cavity. Effect of initial radial misfit between confining ring and specimen is analyzed through computational finite element simulations, and an analytical treatment of problem is also provided to compute the confining stress during elasto-plastic expansion of confining ring. Experimental results suggest that inelastic response of Renew composite is significantly influenced by hydrostatic stress component, and pressure-dependent yield functions are required to analyze plastic deformations and internal damage accumulation process.

Keywords

dental composites; multiaxial loading; interfacial strength; inelasticity; experimental

Introduction

Dental composites are essentially photo-curable polymers reinforced with glass fillers with particle sizes typically spread across nano- and microscales, and they are the most commonly used filling material in modern restorative dentistry. The filler which makes up the bulk of the composite reduces shrinkage of the resin and also further enhances the physical and mechanical properties. Filler particles are typically dispersed in a random fashion within the matrix, making up a composite classified as particulate composite with statistically isotropic properties.1

In dental community, measurement of the strength and fatigue life of dental composites has been heavily based on three-point or four-point flexure testing techniques for decades. For brittle materials such as dental composites, however, flexural strength is governed by the tensile properties of material at the bottom surface of specimen, and it is extremely sensitive to flaws and defects both inherent in the material and introduced during sample preparation, since the tensile failure is dependent upon stress concentrations located at defects in the microstructure. However, as schematically shown in Figure 1, dental composites are

Corresponding author: Murat Vural, Department of Mechanical, Materials, and Aerospace Engineering, Illinois Institute of Technology, 10 West 32nd Street, Chicago, IL 60616, USA vural@iit.edu.

generally set within existing natural tooth as Class I restorations, where the material is subject to axial as well as radial stresses, thereby experiencing a 3D state of compressive stress. Therefore, it is of great interest to experimentally examine the mechanical behavior of dental composites subjected to multiaxial compressive loads, rather than uniaxial compression or tension, as a more clinically relevant means of material testing and in order to develop a better understanding of inelastic deformation and progressive damage mechanisms under realistic loading configurations.

In this study, we place the emphasis on the application of confining ring technique as a means of introducing 3D state of compressive stress in dental composite Renew™. Ma and Ravi-Chandar2 have validated this technique by testing Al 6061-T6 alloy whose multiaxial constitutive behavior is already known. Inelastic deformation of polycarbonate (PC) and polymethylmethacrylate (PMMA) has also been investigated under confined compression by using the same technique.3 However, in these studies, the analytical treatment of technique has been limited to elastic deformations of confining ring. In 'Analysis of confined compression' section, the mechanics of confining ring technique is outlined for both elastic and plastic deformations of the confining ring. We also discuss the effect of initial misfit clearance between the confining ring and the specimen due to machining tolerances and compare experimental results with finite element (FE) simulations. Materials, specimen preparation, and curing time characterization of dental composite is given in 'Experimental' section. A complete experimental characterization of the response of Renew specimens under varying amounts of confining pressure is presented in 'Results and discussion' section.

Analysis of confined compression

In confined compression experiments, the axial stress is applied to specimen through a set of plungers while the lateral expansion of specimen is confined by the confining ring as shown in Figure 2(c). The confining ring can be considered as a thick-walled cylinder subjected to internal pressure, p_c. Thus, the problem becomes a plane axisymmetric one for which the following solution is given for radial and tangential (hoop) stresses, respectively, (e.g., Ref. 4).

$$\sigma_r = \frac{p_c}{\lambda^2 - 1}\left(1 - \frac{r_o^2}{r^2}\right) \tag{1}$$

$$\sigma_\theta = \frac{p_c}{\lambda^2 - 1}\left(1 + \frac{r_o^2}{r^2}\right) \tag{2}$$

where r_o and r_i are the outer and inner radii of the confining ring, respectively, and $\lambda = r_o/r_i > 1$ can be considered as the degree of confinement provided by the ring. We will assume plane stress conditions, that is, $\sigma_z = 0$, dominates within the ring material by neglecting the friction at the specimen–ring interface. The specimen, on the other hand, is exposed to a uniform isotropic in-plane confining stress, $\sigma_r = -p_c$, superposed by the axial loading, σ_z, that is externally applied. Therefore, it is essential to obtain the confinement pressure p_c as it develops during the experiment to fully track the 3D stress state experienced by the specimen. This is conveniently accomplished by measuring the hoop strain on the outer surface of confining ring (Figure 2(c)) and then using Equations (1) and (2) in conjunction with Hooke's law. Thus, from Equation (2) we have:

$$\sigma_\theta^{\text{out}}=\sigma_\theta|_{r=r_o}=\frac{2p_c}{\lambda^2-1} \tag{3a}$$

$$p_c=\frac{\lambda^2-1}{2}\sigma_\theta^{\text{out}} \tag{3b}$$

Hooke's law for plane stress is written as:

$$\varepsilon_\theta=\frac{1}{E^r}(\sigma_\theta-\nu^r\sigma_r) \tag{4}$$

where superscript r denotes properties that belongs to ring material. At the outer surface of ring, that is, when $r = r_o$, the radial stress becomes zero from Equation (1) and the Hooke's law reduces to:

$$\sigma_\theta^{\text{out}}=E^r\varepsilon_\theta^{\text{out}} \tag{5}$$

Thus, Equations (3b) and (5) provides us the following expression that conveniently relates the hoop strain measured at the outer surface of confining ring to the confinement pressure, p_c,

$$p_c=\frac{\lambda^2-1}{2}E^r\varepsilon_\theta^{\text{out}} \tag{6}$$

It is essential to mention at this point that Equation (6) is valid only if the strains in the ring material remain elastic. Therefore, for a particular ring material and geometry, it is essential to calculate the critical hoop strain beyond which plastic deformations invalidate Equation (6). This can be easily done by using maximum shear stress (Tresca) yield criterion, which is both more practical to apply and also gives more conservative results than von Mises yield criterion. Thus, noting that the tangential stress is always positive and radial stress is negative in the confining ring, Tresca yield criterion under plane stress is given by:

$$|\sigma_\theta-\sigma_r|_{\max}=|\sigma_\theta-\sigma_r|_{r=r_i}=\sigma_y^r \tag{7}$$

where, σ_y^r is the yield stress of ring material under uniaxial stress conditions. One immediately notes from Equation (7), the yielding of the ring material initiates at its inner radius. Now, coupling Equation (7) with Equations (1) and (2) gives us the critical confinement pressure as:

$$p_c^*=\frac{\lambda^2-1}{2\lambda^2}\sigma_y^r \tag{8}$$

beyond which plastic deformation starts and the Equation (6) loses its validity. It is also possible to calculate a critical confining pressure by using von Mises yield criterion as follows:

$$p_c^*=\frac{\lambda^2-1}{\sqrt{1+3\lambda^4}}\sigma_y^r \tag{9}$$

One must note that the critical confinement pressure given by Equation (8) is always lower than that of Equation (9) since $\lambda > 1$ and, therefore, the conservative prediction of Tresca criterion, that is, Equation (8), is adopted to monitor the critical stress level during each experiment.

It is essential to test the specimen under different degrees of lateral confinement to understand the effect of stress multiaxiality on its macroscopic mechanical response as well as underlying damage evolution at the microstructural level. Therefore, it would be quite useful to derive an expression that relates confining pressure to axial loading during an experiment as a function of the degree of confinement, λ. Noting that the specimen is under a state of multiaxial stress, generalized Hooke's law in terms of strains and stresses, respectively, is given by:

$$\sigma_{ij}=\frac{E}{1+\nu}\left[\varepsilon_{ij}+\frac{\nu}{1-2\nu}\varepsilon_{kk}\delta_{ij}\right] \tag{10a}$$

$$\varepsilon_{ij}=\frac{1}{E}\left[(1+\nu)\,\sigma_{ij}-\nu\sigma_{kk}\delta_{ij}\right] \tag{10b}$$

Using Equation (10), the axial stress in specimen can be related to confining pressure as follows:

$$\sigma_a=-\frac{E^s}{\nu^s}\left[\frac{1-\nu^s}{E^s}p_c+\varepsilon_r^s\right] \tag{11}$$

The radial strain in specimen, ε_r^s, can be related to the confining pressure by enforcing the compatibility of radial displacements at the interface such that:

$$u^r=u^s \text{ and } \varepsilon_\theta=\frac{u}{r} \quad \therefore \quad \varepsilon_\theta^r=\varepsilon_\theta^s \text{ at } r=r_i \tag{12}$$

The state of isotropic in-plane stress and strain in the specimen further assures that:

$$\varepsilon_r^s=\varepsilon_\theta^s \text{ for } r \le r_i \tag{13}$$

Thus, we can write:

$$\varepsilon_r^s=\varepsilon_\theta^r|_{r=r_i} \tag{14}$$

Now, using Equations (14) and (4) at $r = r_i$ together with Equations (1) and (2), we can write the radial strain in specimen as:

$$\varepsilon_r^s = \frac{p_c}{E^r}\left(\frac{\lambda^2+1}{\lambda^2-1}+\nu^r\right) \tag{15}$$

Then, substituting Equation (15) in Equation (11) and defining the confining stress as $\sigma_c = -p_c$, we get:

$$\frac{\sigma_a}{\sigma_c} = \frac{1}{\nu^s}\left[1+\nu^s+\frac{E^s}{E^r}\left(\frac{\lambda^2+1}{\lambda^2-1}+\nu^r\right)\right] \tag{16}$$

As it is obvious from Equation (16) the relationship between the axial stress and confinement stress depends on the elastic properties of the specimen and confining ring as well as the thickness of confining ring through λ. Thus, before running the confining ring experiment, Equation (16) can be used to estimate the ratio of axial-to-confinement stress or to choose appropriate ring material and its thickness to achieve desired confining pressure. However, one must note that the Equation (16) is valid as long as both the ring and the specimen materials remain elastic.

Elasto-plastic expansion of confining ring

In cases where relatively large inelastic response of the specimen is explored or when the wall thickness of ring is relatively small, the confining ring starts yielding at a critical pressure that can be predicted by using Tresca yield criterion, that is, Equation (8). Once the confining ring starts yielding, the radial location ρ of the boundary between the elastically and plastically deformed zones (elastic–plastic boundary), can be expressed as:

$$\rho = r_o\sqrt{\frac{\varepsilon_\theta^{out}E^r}{\sigma_y^r}} \tag{17}$$

When this situation is reached, the corresponding confining pressure, p_c, becomes:5

$$p_c = \sigma_y^r\left[\ln\frac{\rho}{r_i}+\frac{1}{2}\left(1-\frac{\rho^2}{r_o^2}\right)\right] \tag{18}$$

The maximum confining pressure, for an elastic-perfectly plastic confining ring material, that can be achieved according to Equation (18) is:

$$p_c^{max} = \sigma_y^r \ln\frac{r_o}{r_i} = \sigma_y^r \ln\lambda \tag{19}$$

Thus, Equation (19) describes a constant limiting pressure once the confining ring is fully plasticized. In summary, Equation (6) is used to compute the confining pressure as long as the confining ring remains elastic. When the critical pressure, which is defined by Equations (8) or (9) is reached, the confining ring starts to yield and, then, Equation (18) is used to track the confining pressure until the limiting pressure given in Equation (19) is reached. Thereafter, confining pressure remains constant for an elastic-perfectly plastic ring material. Therefore, Equations (6) and (17) through Equation (19) together with the axial stress fully describe the state of stress in specimen as the confining ring experience elastic, elasto-plastic, and fully plastic deformation fields during loading process.

Contact conditions

One must note that a tight fit between the specimen and confining ring is essential in confining ring experiments. When there is an initial gap between the two, say because of machining tolerances, the specimen will undergo uniaxial compression until it laterally expands enough to come in contact with the confining ring, and that is when the confinement actually starts. We will call this stress as the uniaxial contact stress, σ_a^c. In such situations, it is essential to find out uniaxial contact stress and whether the specimen fails under uniaxial compression before the confinement actually starts, and the results must be evaluated accordingly. Uniaxial contact stress can be calculated in terms of the initial gap δ between the inner surface of confining ring and outer surface of cylindrical specimen (Figure 2) as follows:

$$\varepsilon_r^s = \frac{d_i - d^s}{d^s} = \frac{\delta}{d^s} = -\nu^s \varepsilon_a^s \tag{20}$$

$$\sigma_a^c = -\frac{E^s \delta}{\nu^s d^s} \tag{21}$$

One can also calculate maximum allowable gap δ_{max}, so that the contact is established before the uniaxial stress reaches a certain fraction, α, of uniaxial compressive strength as follows:

$$\delta_{max} = \alpha \sigma_y \frac{\nu^s d^s}{E^s} \tag{22}$$

For example, by using the typical values for dental composite used in this study (σ_y = 120 MPa, ν^s = 0:34, E^s = 6:4 GPa, and d^s = 6:35 mm), one can calculate the maximum allowable gap (δ_{max}) to be around 8 μm (0.0003 in.) in order to establish contact before, say, 20% of uniaxial compressive strength is reached ($\alpha\sigma_y = 0{:}2\sigma_y$). Therefore, in confining ring experiments quite tight tolerances should be used to establish full contact at the early stage of elastic deformation.

Experimental

Materials

Cylindrical specimens were prepared by using Renew and modified Renew composites. Renew (Bisco, Schaumburg, IL) is a commercially available microhybrid dental composite that contains 28% resin and 72% glass filler particles by weight with an average particle size of about 0.7 μm. The matrix is a mixture of bis-GMA (a visible light-cured monomer), tetraethyleneglycol dimethacrylate (TEGDMA), and ethoxyl 2,2-bis(4-methacryloxy phenyl)propane (BPDMA) with mass fractions of 2%, 6%, and 20% of the composite, respectively.6 In order to achieve a consistent matrix with the addition of the particulate filler and to increase the degree of polymerization of the matrix, a lower molecular weight diluent like TEGDMA is added.7 As reported by Zhou et al.,6 the reinforcing phase of Renew composite contains SiO_2, BaO, B_2O_3, and Al_2O_3 particles, and their mass fractions in the composite are given as 43%, 16%, 6.5%, and 6.5%, respectively. The barium glass is added to the composite to provide X-ray opacity to facilitate radiological monitoring of the composite.

The modified Renew composite has been prepared by replacing a fraction of submicron particles (~20%) in original Renew composite with the glass particles of larger size in order to facilitate micromechanical study of the composite before and after mechanical loading. Glass particles with size distribution from 10 to 100 μm were used to prepare a new composite (modified Renew) with the same matrix material as Renew and the same particle mass fraction.

It is widely recognized that good bonding between the matrix and the filler particles is essential, as the interfaces in a composite are potential high stress regions. To ensure this, the filler surface is usually impregnated with a silane coupling agent like 3-(trimethoxysilyl) propyl methacrylate with a chemical formula $C_{10}H_{20}O_5Si$. Therefore, the modified Renew composite was prepared by using silanated filler particles as is the case in original Renew composite. However, an additional set of control specimens were prepared with unsilanated glass particles to study the effect of silane bonds on the interface properties and microstructural damage evolution.

Specimen preparation

In order to capture all details of material behavior under uniaxial and multiaxial compressive loadings as well as for ease of handling and testing we need to mold specimens larger in size than actually used in dental restorations. This reduces the effects of small surface irregularities and potential misalignment complications in experimental setup which can otherwise cause erroneous results. On the other hand, specimen size must be small enough to ensure complete polymerization of the matrix resin under light cure. These considerations led to a cylindrical specimen geometry which is 6.35 mm in diameter and 8 mm in length. A three-piece compression mold was machined from transparent PC and used to prepare cylindrical specimens.

A visible light-curing unit (Dentsply Triad®2000) was used with a 120V/250W tungsten halogen lamp as the light source. The mold with the composite to be cured was placed inside the unit and cured for a certain curing time using the timer on the unit. The table inside the curing unit was allowed to revolve to provide uniform curing from all sides and the mold was also flipped half way through the curing process to ensure complete curing of the specimen from both ends. Before mechanical testing, the flat surfaces of cylindrical specimens were polished by using a custom-made rig to ensure that the surfaces are exactly parallel to each other with a good surface finish and also to ensure perfect contact between the specimen and loading plungers.

Curing time characterization

It is well established that the degree of polymerization and the depth of cure may vary as a function of the type of light source, its power intensity, and time of exposure.[8-10] Hardness test has been the most popular method for investigating factors that influence the degree of conversion of composite resins.[11,12] It has been reported that this test provides an estimation of the degree of conversion of a composite resin.[9] Although the hardness values cannot be used to directly compare the conversion of different composites, the bottom/top ratios for both hardness and degree of conversion results in a linear relationship independent of filler size or loading.[13] Therefore, in order to ensure that the specimens are uniformly and completely cured under the light source used in this study, a series of Vickers micro-hardness tests have been performed at 10 points along the diameter of specimens at central cross-sectional plane after subjected to varying amounts of light exposure between 1 and 15 min. The results show that hardness is quite uniform across the diameter of cylindrical specimens within ±3 pct of the average hardness value for all curing times. It is obvious from the variation of this average hardness plotted in Figure 3 that 10 min of light exposure

fully cures the specimens. Therefore, all specimens used in mechanical tests have been cured for 10 min.

A few tensile experiments were also performed with dog-bone specimens subjected to different curing times to validate the results of the micro-hardness tests as well as determine the Young's modulus and Poisson's ratio of fully cured composite. A new mold was machined, and tensile specimens were molded in accordance with Type-IV specimen geometry described in 'ASTM D638-98 standard test method for tensile properties of plastics'. The tensile experiments were conducted by using an Instron Universal Tensile Testing Machine with a 1000-lb load cell and an extensometer with 25.4 mm gage length. To ensure there was no misalignment in the loading configuration causing bending of the specimen, two strain gages were glued along the gage length of the specimen on the opposite faces to monitor if the deformation of the specimen was uniform and equal on both faces. For the measurement of Poisson's ratio, a T-gage was glued at the center of the gage length to record strains in both longitudinal and transverse directions. Figure 4 shows the stress–strain response in tension until the specimen ruptures. It is obvious from these plots that the Young's modulus of modified Renew composite increases with increase in curing time, while strain to failure decreases. It can also be observed that the Young's modulus of fully cured matrix resin is much lower than that of the composite. The resin, being a polymer, exhibits comparatively much larger deformation before failure. The Young's modulus and Poisson's ratio of the Renew composite cured for 10 min were measured to be 20 GPa and 0.34, respectively, from uniaxial tension experiments. On the other hand, Young's modulus of the same composite in compression was measured to be 6.6 GPa after 10 min curing, which is lower by a factor of three than the one in tension.

Experimental setup for confining ring experiments

The experimental setup of confining ring technique including the specimen, Al 7075-T6 confining ring and high-strength plungers made of 17-4 PH stainless steel is shown in Figure 2(c). Here, extreme care was taken to ensure that the gap between the specimen and the confining ring was minimal for a snug fit. After curing the specimen seemed to shrink, and the diameter was 6.3 mm instead of 6.35 mm. Therefore, confining rings and plungers were machined with an internal diameter of 6.3 mm to maintain close tolerances between mating surfaces. The cross-head speed during compressive loading was kept constant at 0.254 mm/min, giving a strain rate of about $5 \times 10^{-4} s^{-1}$. The specimen assembly was placed in the compression fixture, and a pre-calibrated linear variable differential transformer (LVDT) was used to measure axial displacement. The hoop strain in the confining ring was measured through a strain gage in quarter-bridge configuration glued on the outer surface of the confining ring as shown in Figure 2(c). Confining rings have been machined from Al 7075-T6 alloy for two reasons. The first is that this particular alloy has a high yield stress, which is 550 MPa, so that we can use the elastic relations (such as Equations (6) and (16)) for an extended range of axial deformation. The second reason is that Al 7075-T6 alloy has an almost non-hardening plastic flow stress so that Equations (17)-(19) can be conveniently used to calculate the evolution of confining pressure during elasto-plastic expansion regime of ring material.

Results and discussion

Confined vs. uniaxial compression

The evolution of axial stress and confining stress in Renew composite is shown in Figure 5 as a function of axial strain for $\lambda = 1.25$. Stress–strain curve under uniaxial compression is also plotted in Figure 5 for a direct comparison of results. In this particular example, the confining stress does not start developing right from the beginning with the axial stress, but

rather it starts increasing after a short delay because of an initial gap between the specimen and confining ring as discussed in 'Contact conditions' section. Due to this initial gap, axial compression of specimen starts in an unconfined state and follows the same linear path as uniaxial compression experiment. As the axial stress rises, the Poisson expansion in transverse direction eventually brings the specimen surface in contact with confining ring at which point confining stress starts increasing as well. The plots suggest that for this particular example, the contact is established when the axial stress reaches about 35 MPa. As it is obvious from the plots in Figure 5, the rate of increase in axial stress exhibits a sudden change at this point and starts deviating from uniaxial compressive response, which is taken as further evidence that the contact is established at about 35 MPa. Once the contact is established, the state of stress in specimen transitions from uniaxial to multiaxial compression, and the specimen can sustain much higher axial stress under confined compression than corresponding uniaxial (unconfined) compression. In parallel to axial stress, confining stress also increases with axial strain. When the confining stress reaches a critical level discussed in 'Analysis of confined compression' section (which is 99 MPa for this particular experiment), the ring material starts yielding at the inner surface and plastic deformation zone propagates toward outer surface with further axial strain. During this elasto-plastic expansion regime, which corresponds to axial strains between 0.053 and 0.064, Equation (18) is used to calculate the confining stress. Once the plastic zone completely spreads over the ring material, maximum confining pressure given by Equation (19) is used to calculate constant limiting pressure applied by ring on the specimen (which is 123 MPa for $\lambda = 1.25$). It must be noted that the Renew composite shows a catastrophic failure when the axial strain reaches 0.1 in uniaxial compression experiments, while the same dental composite can sustain higher strains without any sign of catastrophic failure under confined compression.

FE analysis and effect of initial gap

As discussed in 'Contact conditions' section and further exemplified in preceding section, the confining ring experiments require tight tolerances in machining confining rings to establish full contact at the early stage of elastic loading. To assess the potential impact of initial gap on experimental results, we performed a series of FE simulations of the confining ring experiments, where we parametrically changed the amount of initial gap, δ, given by Equation (20).

The FE mesh was generated using Hypermesh and the computations were carried out using the ABAQUS solver. The specimen and confining ring were both meshed using 8-node brick elements, with finer mesh size in the vicinity of interface to improve simulation accuracy at the contact surface. A surface-based contact technique was used to simulate surface interaction between the specimen and the confining ring. Although a frictional surface interaction was defined for contacting surfaces, the friction coefficient was set to zero based on the assumption of good interface lubrication. An elastic-perfectly plastic constitutive model was used for the ring material with Young's modulus 72 GPa and yield stress 550 MPa that represent the material properties of Al 7075-T6 alloy used in experiments. Experimental uniaxial stress–strain curve of Renew composite was used to define the constitutive response of specimen (see the thick solid curve in Figure 5). Thus, the specimen was modeled as linear elastic with a Young's modulus of 6.6 GPa, and then to simulate plasticity, the experimental stress–strain data of the composite were provided in the ABAQUS *.inp file. ABAQUS then fits a curve through the provided stress–strain data which provides the required material's non-linearity in plastic regime.

Results of FE analysis are presented in Figure 6 for varying amounts of initial gap, i.e., for $\delta = 0$, 5, 15, 25, and 50 μm. In this simulation, $\lambda = 1.25$ is chosen for confining ring geometry. Solid lines in the graph represents the axial stress applied on the specimen, while dashed

lines show the evolution of confining stress. As the initial gap between the specimen and confining ring increases, the establishment of contact is delayed, and this can significantly alter the evolution of axial stress and underlying deformation mechanism when δ becomes larger such as 50 μm. Therefore, FE analysis also confirms that quite tight tolerances must be maintained in confining ring experiments to establish full contact at the early stage of elastic deformation.

Effect of confining pressure

Figure 7 shows a typical comparison of experimental results with the ones obtained from FE analysis for $\lambda = 1.5$ and an initial gap of $\delta = 5$ μm. The FE prediction of confining stress is very close to experimentally measured one, but there is still slight difference apparently due to a slightly larger initial gap in experiment than 5 μm, but not as much as 15 μm. Maximum confining stress calculated from experimental data through Equation (19) is also noted to be slightly lower than that of FE analysis. Although small, this difference stems from the fact that FE analysis uses J2 (Mises) flow rule to compute incremental plastic deformations, while we adopted more conservative Tresca yield criterion in the derivation of Equation (19) for simplicity.

On the other hand, axial stress measured in experiments significantly differs from FE predictions after the plastic yielding starts in specimen (Figure 7). Following the onset of plastic deformation, experimentally measured axial stress gradually becomes higher than FE prediction. This observation remains the same for all the three confinement levels investigated in this study, that is, for $\lambda = 1.25$,1.5, and 2.0. Furthermore, as the confinement pressure increases with λ, the difference between experimentally measured axial stress and that predicted from FE analysis also increases, suggesting a pressure-dependent plastic flow behavior in Renew dental composite. Once again, one must be reminded that the constitutive behavior of specimen was modeled as an elastic-hardening plastic in FE analysis without any pressure sensitivity. Therefore, any specimen material with inherent pressure sensitivity in its plastic flow behavior would generate such a difference in axial stress observed in Figure 7. In fact, since the confining ring technique allows concurrent measurement of 3D stress state experienced by the specimen, it can be effectively used to determine pressure sensitivity of dental composites and develop pressure-dependent yield functions, which will be the subject of a future work.

An overall picture of the effect of confining pressure on the axial response of Renew composite is shown in Figure 8. These results suggest that increasing the amount of confinement delays the onset of plasticity as well as failure strain and also results in a stiffer response along with smaller strains for a given stress level. From the clinical point of view, this translates into a better life expectancy in smaller Class I dental restorations because the smaller the restorative filling gets, the larger the amount of lateral confinement gets, and this results in higher confining pressure for a given axial stress and smaller axial strain.

Effect of interface strength

It is widely recognized that surface treatment of particles such as salination improves the bonding strength between reinforcing glass fillers and matrix resin. In order to observe the effect of surface treatment, we prepared two sets of modified Renew composites; one with unsalinated (as is) and the other with salinated glass particles as described in ‘Materials’ section. Micrographs in Figure 9(a) and (b) shows the crack paths in unconfined and confined specimens loaded up to 8% strain (where it failed) and 11% strain, respectively, for unsalinated particles. It is clear from the micrographs that when the crack reaches an unsalinated particle it deviates from its path and follow the weak interface around the particle causing interface debonding. The absence of saline bonds between the filler and the

matrix results in a weak interface. Thus, when a propagating crack reaches a particle and loads it, the interface fails first and the crack propagates further into the matrix without shearing or crushing the glass particles. On the other hand, similar micrographs shown in Figure 9(c) and (d) for modified Renew with salinated particles do not show any sign of interface debonding. In this case, interface bonding seems to be so strong that the crack propagates by shearing through the particles. Comparison of Figure 9(c) with (d) is particularly noteworthy as the latter clearly shows the effect of high confining pressure in shearing process. Increased white contrast in Figure 9(d) along the crack path shows the local shear-assisted crushing of glass particles under pressure as the crack propagates. Also, note that under confined compression in Figure 9(d) crack seems to be completely closed due to existence of significant hydrostatic stress component, while one can observe a visible crack opening in Figure 9(c) under unconfined uniaxial compression. These results suggest that the surface treatment of filler particles plays an important role in microstructural failure mechanism within the dental composite through its effect on interface strength. The interface is always a high stress region and is usually the region from which the cracks originate.

Conclusions

Mechanical response of a photo-curable dental composite (Renew) has been characterized under uniaxial tension and compression as well as multiaxial stress states *via* confining ring experiments. Due to larger size of specimens used, relative to typical sizes used in dental restorations, the variation of micro-hardness and tensile Young's modulus as a function of curing time has been investigated to achieve full curing. The results show that curing beyond 10 min does not cause any further increase in micro-hardness or tensile Young's modulus. Surprisingly, experimental results for fully cured specimens show that Young's modulus in compression (6.6 GPa) is by a factor three lower than the one in tension (20 GPa). This discrepancy is attributed to complex interaction between applied far field stress and dominantly compressive residual stress field in the microstructure. This constitutes an interesting problem that deserves further study.

Dental composites used in Class I restorations are subjected to a state of 3D compressive stress during the application of masticatory forces in oral cavity. The confining ring technique, which can realistically mimic this multiaxial stress state, has been described and proposed as a practical experimental tool as well as a more clinically relevant means of material testing to investigate and better understand the mechanical response and progressive damage mechanisms in restorative dental composites. Data reduction procedure has been outlined for elastic, elasto-plastic, and fully plastic expansion regimes of confining ring to track the evolution of confining stress throughout an experiment. Implications of practical issues such as the effect initial gap between the test specimen and confining ring have also been discussed with the aid of FE analysis, and it is concluded that tight machining tolerances are required for all the components used in confining ring experiments. Comparison of experimental results with FE simulations suggests that inelastic deformation behavior of dental composites can be described as pressure-dependent because the axial stresses calculated in FE analysis by using J2 (Mises) flow rule significantly underestimate experimental values when hydrostatic component of stress is increased. This observation calls for further study on the pressure-dependent response of dental composites, and the confining ring technique stands out as the perfect tool for such a study.

Acknowledgments

We are grateful for the support provided through NIDCR grant HHS DE07979. We also thank Bisco Inc. for supplying the dental composite.

References

1. Hashin Z. Analysis of composite materials – a survey. J Appl Mech. 1983; 50:481–505.
2. Ma Z, Ravi-Chandar K. Confined compression: a stable homogeneous deformation for constitutive characterization. Exp Mech. 2000; 40(1):38–45.
3. Ravi-Chandar K, Ma Z. Inelastic deformation in polymers under multiaxial compression. Mech Time-Depend Mater. 2000; 4:333–357.
4. Ragab, A-R.; Bayoumi, SE. Engineering solid mechanics: fundamentals and applications. CRC Press; Boca Raton, FL: 1999.
5. Cook, RD.; Young, WD. Advanced mechanics of materials. 2nd ed. Prentice-Hall Inc; Upper Saddle River, NJ: 1999.
6. Zhou M, Drummond JL, Hanley L. Barium and strontium leaching from aged glass particle/resin matrix dental composites. Dent Mater. 2005; 21:145–155. [PubMed: 15681013]
7. Arcis RW, Lopez-Macipe A, Toledano M, et al. Mechanical properties of visible light-cured resins reinforced with hydroxyapatite for dental restoration. Dent Mater. 2002; 18:49–57. [PubMed: 11740964]
8. Cook WD. Factors affecting the depth of cure of UV-polymerized composites. J Dent Res. 1980; 59(5):800–808. [PubMed: 6928870]
9. Ferracane JL. Correlation between hardness and degree of conversion during the setting reaction of unfilled dental restorative resins. Dent Mater. 1985; 1:11–14. [PubMed: 3160625]
10. Leung RL, Fan PL, Johnston W. Post-irradiation polymerization of visible-light-activated composite resins. J Dent Res. 1983; 62(3):363–365.
11. Obici AC, Sinhoreti MAC, Sobrinho LC, de Gose MF, Consani S. Evaluation of depth of cure and Knoop hardness in a dental composite photo-activated using different methods. Braz Dent J. 2004; 15(3):199–203. [PubMed: 15798823]
12. Thome T, Steagall W Jr, Tachibana A, Braga SRM, Turbino ML. Influence of the distance of the curing light source and composite shade on hardness of two composites. J Appl Oral Sci. 2007; 15(6):486–491. [PubMed: 19089185]
13. Bouschlicher MR, Rueggeberg FA, Wilson BM. Correlation of bottom-to-top surface microhardness and conversion ratios for a variety of resin composite compositions. Oper Dent. 2004; 29:698–704. [PubMed: 15646227]

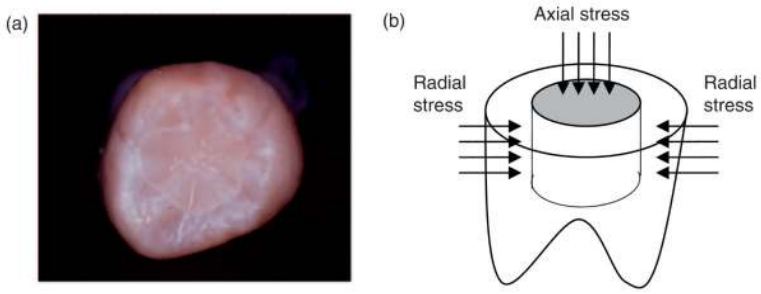

Figure 1.
(a) Class I composite restoration and (b) Class I restoration placed in tooth experiences axial and radial stresses.

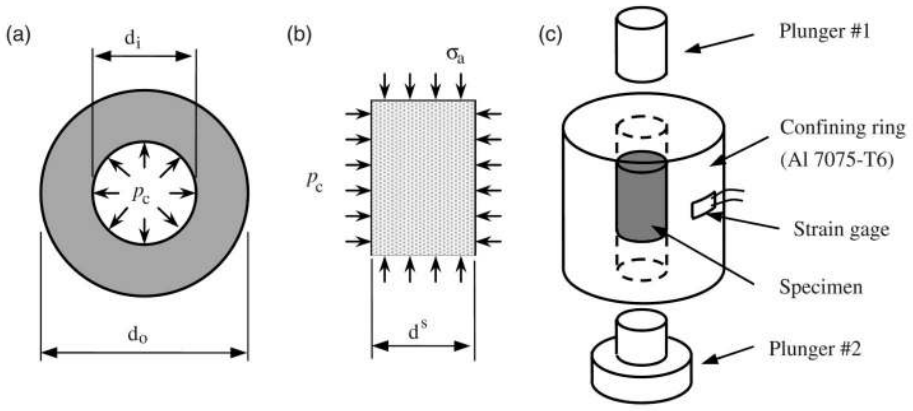

Figure 2.
Schematics of confining ring configuration: (a) hollow confining ring, (b) cylindrical test specimen, and (c) assembly.

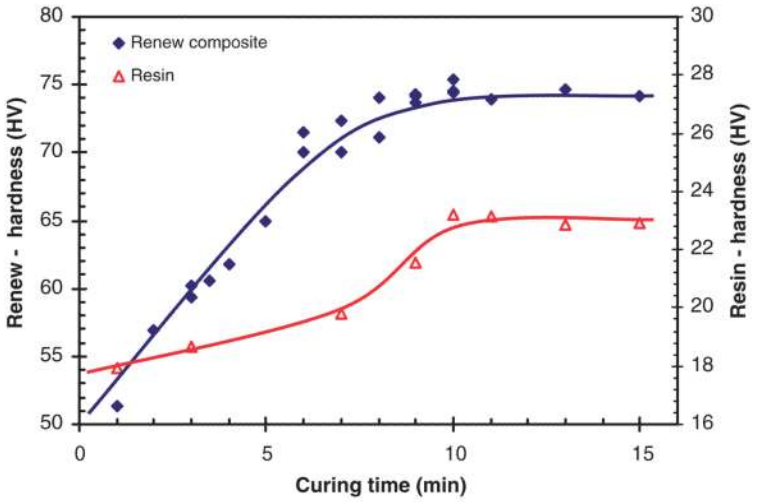

Figure 3.
Variation of micro-hardness in Renew composite and resin as a function of curing time.

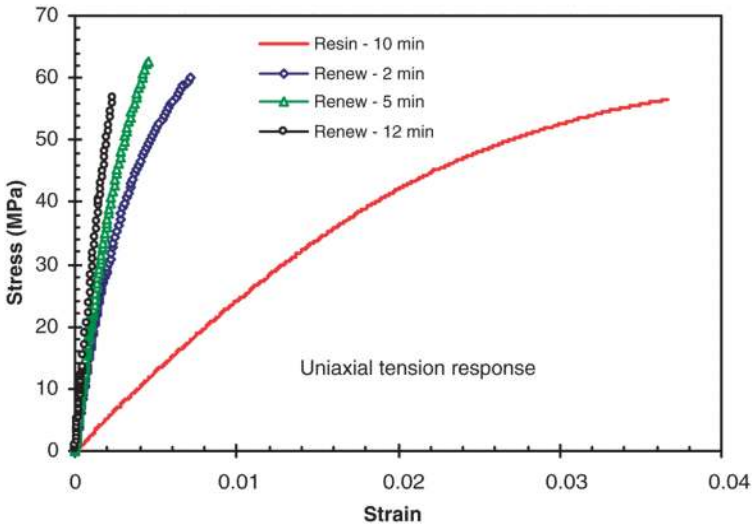

Figure 4.
Uniaxial tensile response of matrix resin and Renew composite for various curing times.

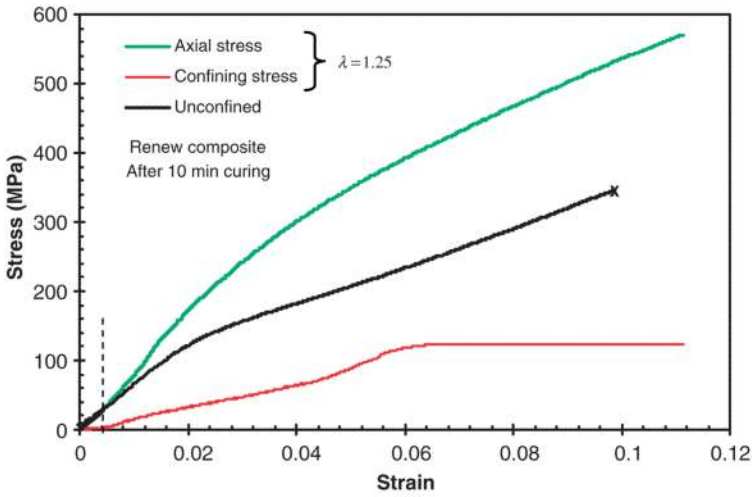

Figure 5.
Evolution of axial and confining stresses in confined compression experiments ($\lambda = 1.25$) for Renew composite as compared to its uniaxial unconfined response.

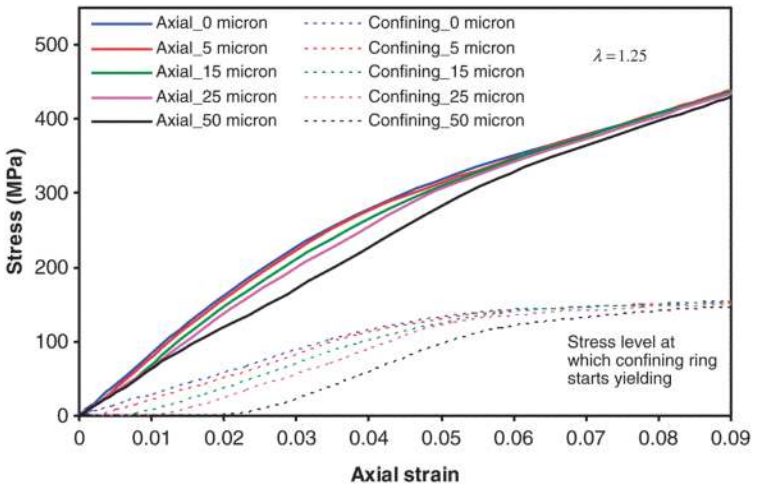

Figure 6.
The effect of a gap 'δ' between the specimen and the confinement ring on the development of axial and confinement stresses in the specimen for $\lambda = 1.25$.

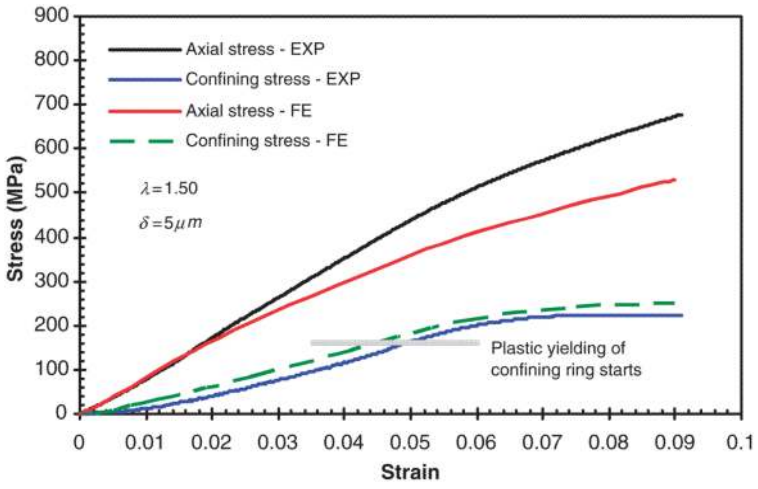

Figure 7.
Comparison of stress–strain response from FE simulation and confining ring experiments for $\lambda = 1.25$ and $\delta = 5$ μm.

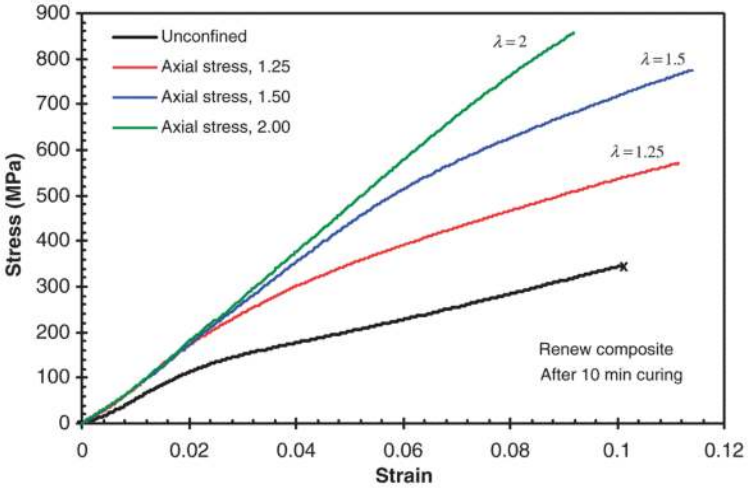

Figure 8.
Effect of confinement on the stress–strain response of Renew composite.

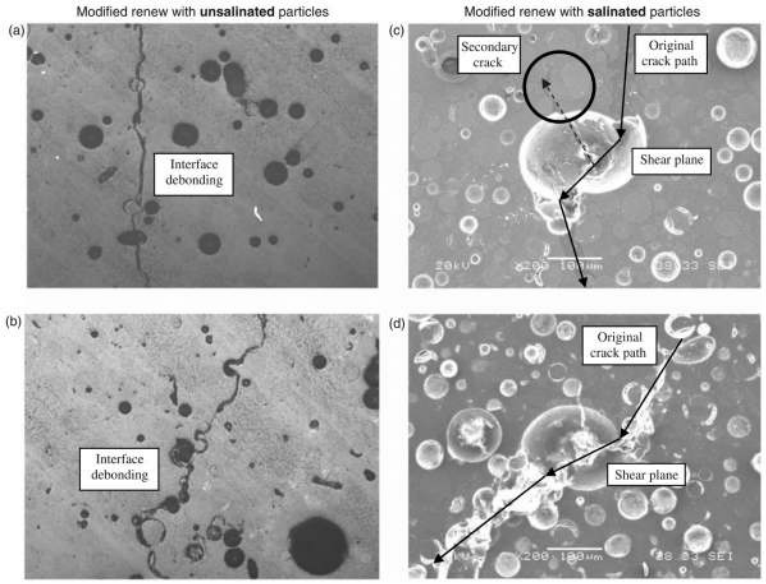

Figure 9.

Micrographs show examples of interface debonding and particle shearing in modified Renew composite with unsalinated (left column) and salinated (right column) glass particles, respectively, under both uniaxial compression and confined compression experiments. (a) Unconfined, failed at $\varepsilon_a = 0.08$, (b) confined $\lambda = 1.25$, unloaded at $\varepsilon_a = 0.11$, (c) unconfined, failed at $\varepsilon_a = 0.06$, (d) confined $\lambda = 1.25$, unloaded at $\varepsilon_a = 0.09$.